Hindawi Publishing Corporation
Journal of Nanomaterials
Volume 2015, Article ID 854840, 8 pages
http://dx.doi.org/10.1155/2015/854840

Research Article

Mössbauer Spectroscopy, Structural and Magnetic Studies of Zn^{2+} Substituted Magnesium Ferrite Nanomaterials Prepared by Sol-Gel Method

Yun He,[1] Xingxing Yang,[1] Jinpei Lin,[1] Qing Lin,[1,2] and Jianghui Dong[3]

[1]*College of Physics and Technology, Guangxi Normal University, Guilin 541004, China*
[2]*Department of Information Technology, Hainan Medical College, Haikou 571101, China*
[3]*School of Natural and Built Environments, University of South Australia, Adelaide, SA 5095, Australia*

Correspondence should be addressed to Qing Lin; hy@gxnu.edu.cn

Received 8 August 2014; Accepted 26 August 2014

Academic Editor: Xinqing Chen

Zinc substituted magnesium ferrite nanomaterials $Mg_{1-x}Zn_xFe_2O_4$ (x = 0, 0.1, 0.3, 0.5, 0.7) powders have been prepared by a sol-gel autocombustion method. The lattice parameter increases with increase in Zn concentration, but average crystallite size tends to decrease by increasing the zinc content. SEM results indicate the distribution of grains and morphology of the samples. Some particles are agglomerated due to the presence of magnetic interactions among particles. Room temperature Mössbauer spectra of $Mg_{1-x}Zn_xFe_2O_4$ shows that the A Mössbauer absorption area decreases and the B Mössbauer absorption area increases with zinc concentration increasing. The change of the saturation magnetization can be explained with Néel's theory. It was confirmed that the transition from ferrimagnetic to superparamagnetic behaviour depends on increase in zinc concentration by Mössbauer spectra at room temperature. Saturation magnetization increases and coercivity decreases with Zn content increasing.

1. Introduction

Magnesium ferrite is a soft magnetic n-type semiconducting material, which is used in catalysis, gas sensors, transformers, ferrofluids, fuel cells, and magnet core of coils [1, 2]. It has been reported [3, 4] that the structure of magnesium ferrite is partially inverse spinel, with 0.1 of Mg^{2+} ions and 0.9 of Mg^{2+} ions distributed over the A and B sites in the following way $(Mg_{0.1}Fe_{0.9})[Mg_{0.9}Fe_{1.1}]O_4$. The magnetic properties of nonmagnetic Zn substituted ferrites have attracted considerable attention because of the importance of these materials for high-frequency applications [5, 6]. Zinc ferrite possesses a normal spinel structure, and all Zn^{2+} ions reside on tetrahedral A sites. Therefore, substitution of Mg by Zn in $Mg_{1-x}Zn_xFe_2O_4$ is expected to increase the magnetic moment up to a certain limit; thereafter, it decreases for the canting of spins in octahedral B sites. Choodamani et al. [7] investigated thermal effect on magnetic properties of Mg-Zn ferrite nanoparticles, and magnetic properties were found to be affected by particle size. In this paper, ferrite $Mg_{1-x}Zn_xFe_2O_4$ (x = 0, 0.1, 0.3, 0.5, 0.7) powders were prepared by a sol-gel autocombustion method. The aim of this study is to investigate variation structural and magnetic properties of magnesium ferrite powders by partial replacement of nonmagnetic zinc cations.

2. Experimental

2.1. Sample Preparation. Zinc substituted magnesium ferrite $Mg_{1-x}Zn_xFe_2O_4$ (x = 0, 0.1, 0.3, 0.5, 0.7) powders were prepared by a sol-gel autocombustion method. The analytical grades $Mg(NO_3)_2{\cdot}6H_2O$, $Zn(NO_3)_2{\cdot}6H_2O$, $Fe(NO_3)_3{\cdot}9H_2O$, citric acid ($C_6H_8O_7{\cdot}H_2O$), and ammonia ($NH_3{\cdot}H_2O$) were used as raw materials. The molar ratio of metal nitrates to citric acid was taken as 1 : 1. The metal nitrates and citric acid were, respectively, dissolved into deionized water to form solution. The solution of metal nitrates was added to ammonia to change the pH value from 7 to 9. The mixed solution was poured into a thermostat water bath and heated at 80°C under constant stirring to transform into a dried gel.

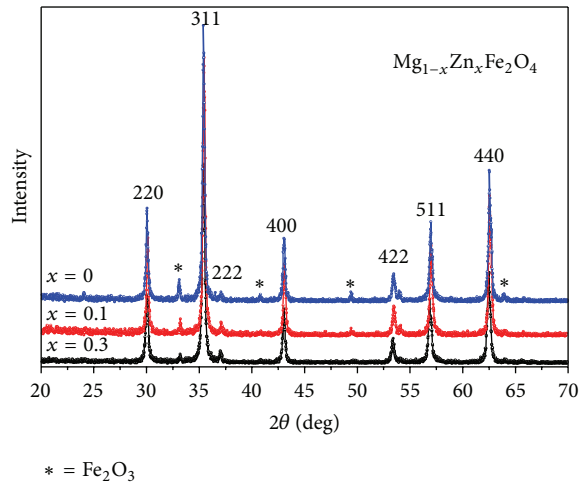

Figure 1: Room temperature X-ray diffraction patterns of $Mg_{1-x}Zn_xFe_2O_4$ annealed at 800°C.

Citric acid was dropped continually in the process of heating. The gel was dried at 120°C in a dry oven for 2 h and, being ignited in air at room temperature, the dried gel burnt in a self-propagating combustion way to form loose powder. The powder was ground and annealed at temperature of 800°C for 3 h.

2.2. Characterization. The crystalline structure was investigated by X-ray diffraction (D/max-2500V/PC, Rigaku) with Cu K_α radiation ($\lambda = 0.15405$ nm). The micrographs were obtained by scanning electron microscopy (NoVa Nano SEM 430). The Mössbauer spectrum was performed at room temperature (25°C), using a conventional Mössbauer spectrometer (Fast Com Tec PC-moss II), in constant acceleration mode. The γ-rays were provided by a ^{57}Co source in a rhodium matrix. Magnetization measurements were carried out with super conducting quantum interference device (MPMS-XL-7, Quantum Design) at room temperature.

3. Results and Discussion

3.1. XRD Patterns Analysis. Figure 1 shows the XRD patterns of $Mg_{1-x}Zn_xFe_2O_4$ ($x = 0$, 0.1, 0.3) ferrites calcined at 800°C for 3 h. The impurity peak of Fe_2O_3 is detected in the samples with $x = 0$, 0.1 and 0.3, and increasing the content of Zn is favorable for the synthesis of pure Mg-Zn ferrites. Similar results also were reported in the other literature [6].

Table 1 indicates that the lattice constant increases with the increasing substitution of Zn^{2+} ions. The increase in lattice parameter is probably due to replacement of smaller Mg^{2+} ions (0.72 Å) by larger Zn^{2+} ions (0.74 Å) [8, 9].

The X-ray density was calculated using the relation [4, 10, 11]:

$$\rho_x = \frac{8M}{Na^3}, \quad (1)$$

where M is relative molecular mass, N is Avogadro's number, and "a" is the lattice parameter. Table 1 shows the X-ray density increase with Zn^{2+} concentration for all samples. The atomic weight of Zn is greater than that of Mg, so the relative molecular mass increases with Zn concentration increasing. The increase in X-ray density is attributed to the fact that relative molecular mass increases more than the negligible rise of the lattice parameter.

Table 1: Lattice parameters, average crystallite size, and X-ray densities date of $Mg_{1-x}Zn_xFe_2O_4$ annealed at 800°C.

Sample (x)	Lattice parameter (Å)	Average crystallite size (Å)	Density ($g \cdot cm^{-3}$)
0	8.39786	411	4.4859
0.1	8.39491	356	4.5829
0.3	8.40864	322	4.7440
0.5	8.43133	377	4.8879
0.7	8.43576	385	5.0620

The average crystallite size of the investigated samples estimated by Scherrer's formula [10–12] is found to be around 32~41 nm. The slight decrease in the crystallite size by the addition of Zn indicates that the presence of zinc obstructs the crystal growth [13, 14].

3.2. Structures and Grain Sizes. The SEM micrographs of $MgFe_2O_4$ annealed 800°C for 3 h are shown in Figure 2. The distribution of grains with almost uniform size can be observed. Figure 3 shows the histogram of grain size distribution of $MgFe_2O_4$ ferrites. The average grain size of $MgFe_2O_4$ is approximately 96.26 nm by using a statistical method. The average grain size is slightly larger than the average crystallite size determined by XRD.

The SEM micrographs of $Mg_{0.5}Zn_{0.5}Fe_2O_4$ annealed 800°C for 3 h are shown in Figure 4. The distribution of grains with almost uniform size can be observed, well crystallized for $Mg_{1-x}Zn_xFe_2O_4$ ($x = 0.5$). Some particles are agglomerated due to the presence of magnetic interactions among particles [14].

Figure 5 shows the histogram of grain size distribution of $Mg_{0.5}Zn_{0.5}Fe_2O_4$ ferrites. The average grain size of $Mg_{0.5}Zn_{0.5}Fe_2O_4$ ($x = 0.5$) is approximately 90.74 nm by using a statistical method. It shows that the ferrite powers are nanoparticles, and the average grain size decreases with Zn content increasing. This shows that every particle is formed by a number of crystallites [15, 16].

3.3. Mössbauer Spectroscopy. The Mössbauer spectra recorded at room temperature are shown in Figure 6 for $Mg_{1-x}Zn_xFe_2O_4$. All samples have been analyzed using Mösswinn 3.0 program. For the $Mg_{1-x}Zn_xFe_2O_4$ with $x = 0, 0.1$, the spectra exhibit two normal Zeeman-split sextets due to Fe^{3+} at tetrahedral and octahedral sites, indicating the ferromagnetic behavior of the samples.

The sextet with the larger isomer shift is assigned to the Fe^{3+} ions at the B site and the one with the smaller isomer shift is assumed to arise from the Fe^{3+} ions occupying the A site. May be it is due to difference in Fe^{3+}–O^{2-} internuclear separation. Compared with A site ions, the bond separation

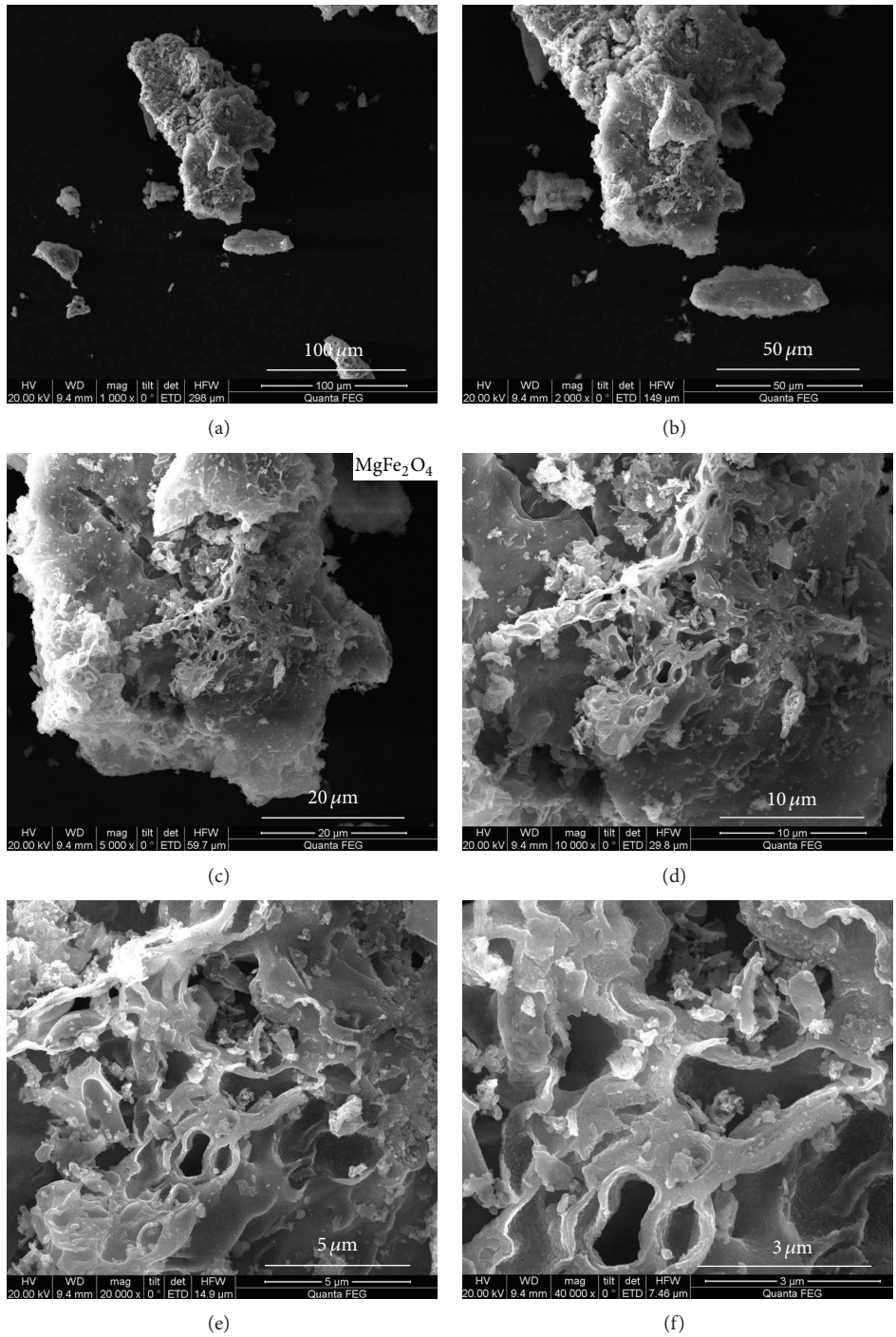

Figure 2: SEM micrographs depict $MgFe_2O_4$ ferrites with diameters of 100 μm (a), 50 μm (b), 20 μm (c), 10 μm (d), 5 μm (e), and 3 μm (f).

is larger for B site Fe^{3+} ions. In addition, overlap-ping of orbit is smaller for Fe^{3+} and O^{2+} ions at B site, which results in smaller covalency and larger isomer shift for Fe^{3+} ions at B site [17, 18]. It is reported that the values of IS for Fe^{2+} ions lie in the range 0.6~1.7 mm/s, while for Fe^{3+} they lie in the range 0.1~0.5 mm/s [19]. From Table 2, values for IS in our study indicate that iron is in Fe^{3+} state.

Table 2 shows the values of magnetic hyperfine field at A and B sites decrease by increasing nonmagnetic zinc substitution. The value of quadrupole shift of the A and B magnetic sextets is very small in the samples indicating that the local symmetry of the ferrites obtained is close to cubic [20]. The A Mössbauer absorption area decreases and the B Mössbauer absorption area increases with increasing zinc

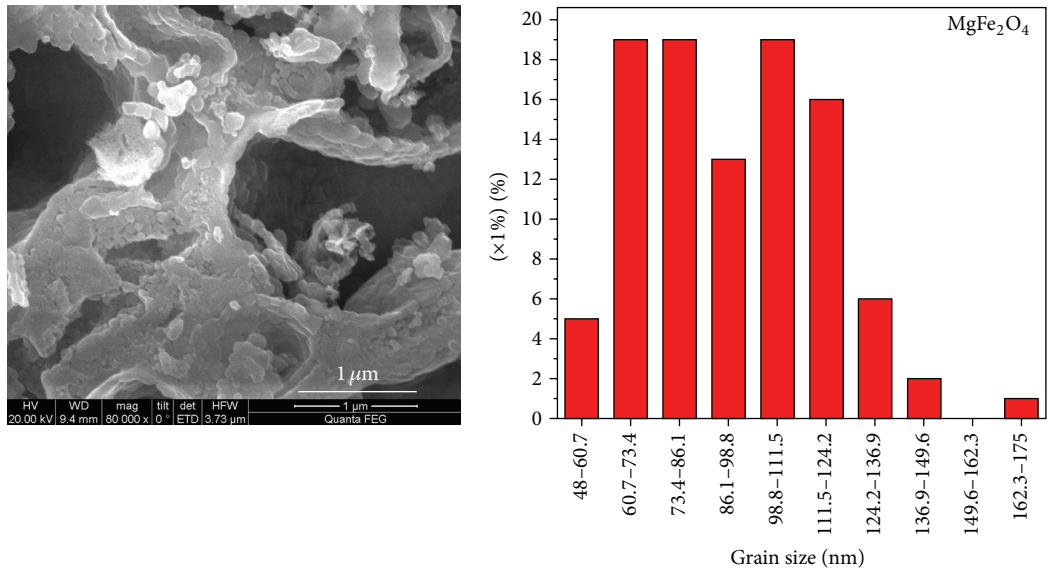

Figure 3: Histogram of grain size distribution of $MgFe_2O_4$ ($x = 0$) annealed at 800°C.

Table 2: Mössbauer parameters of isomer shift (IS), quadrupole splitting (QS), magnetic hyperfine field (H), line width (Γ), and absorption area (A_0) for $Mg_{1-x}Zn_xFe_2O_4$ annealed at 800°C.

Sample (x)	Component	IS (mm/s)	QS (mm/s)	H (T)	Γ (mm/s)	A_0 (mm/s)
0	Sextet (A)	0.163	0.011	45.871	0.503	17
	Sextet (B)	0.332	0.032	43.306	0.325	83
0.1	Sextet (A)	0.224	0.077	45.059	0.473	15
	Sextet (B)	0.294	−0.028	41.322	0.313	85
0.3	Sextet (B)	0.291	−0.009	34.072	0.363	100
0.5	Sextet (B)	0.318	0.005	24.234	0.268	100
0.7	Double	0.336	0.472	—	0.357	100

concentration, since Zn^{2+} substitutes Mg ferrite and occupies the A site, leading to transfer of Fe^{3+} from A site to B site.

When $x = 0.3, 0.5$, the spectra of $Mg_{1-x}Zn_xFe_2O_4$ are only the B magnetic sextet, and the magnetic sextet of A site vanishes which indicates the presence of Fe^{3+} ions only in the octahedral B site [21]. The spectrum obtained for the composition with $x = 0.5$ shows features of relaxation effects and was analyzed to a single sextet. Mössbauer spectra for the samples with $x = 0.7$ consist only of a central doublet, and it exhibits superparamagnetic character. The central doublet can be attributed to the magnetically isolated Fe^{3+} ions which do not participate in the long-range magnetic ordering due to a large number of nonmagnetic nearest neighbors [20, 21].

3.4. Magnetic Property of Particles. Figure 7 shows hysteresis loops of $Mg_{1-x}Zn_xFe_2O_4$ at room temperature. The magnetization of all samples nearly reaches saturation at the external field of 5000 Oe. It is observed from Table 3 that saturation magnetization increases as Zn content x increases. The saturation magnetization could be expressed by means of the following relation [22, 23]:

$$\sigma_s = \frac{5585 \times n_B}{M}, \quad (2)$$

where n_B is magnetic moment with Bohr magneton as the unit and M is relative molecular mass. The relative molecular mass of $Mg_{1-x}Zn_xFe_2O_4$ decreases as Zn content x increases.

The change of magnetic moment n_B can be explained with Néel's theory. The magnetic moment for Zn^{2+}, Mg^{2+}, and Fe^{3+} ions is $0_{\mu B}$, $0_{\mu B}$, and $5_{\mu B}$, respectively [3, 4]. According to Néel's two sublattice model of ferrimagnetism, using the cation distribution of $(Zn_xMg_yFe_{1-x-y})[Mg_{1-x-y}Fe_{1+x+y}]O_4$, since Zn^{2+} ions have a stronger preference for the tetrahedral sites [11, 12], and Mg^{2+} ions exist in both sites but have a preference for the octahedral

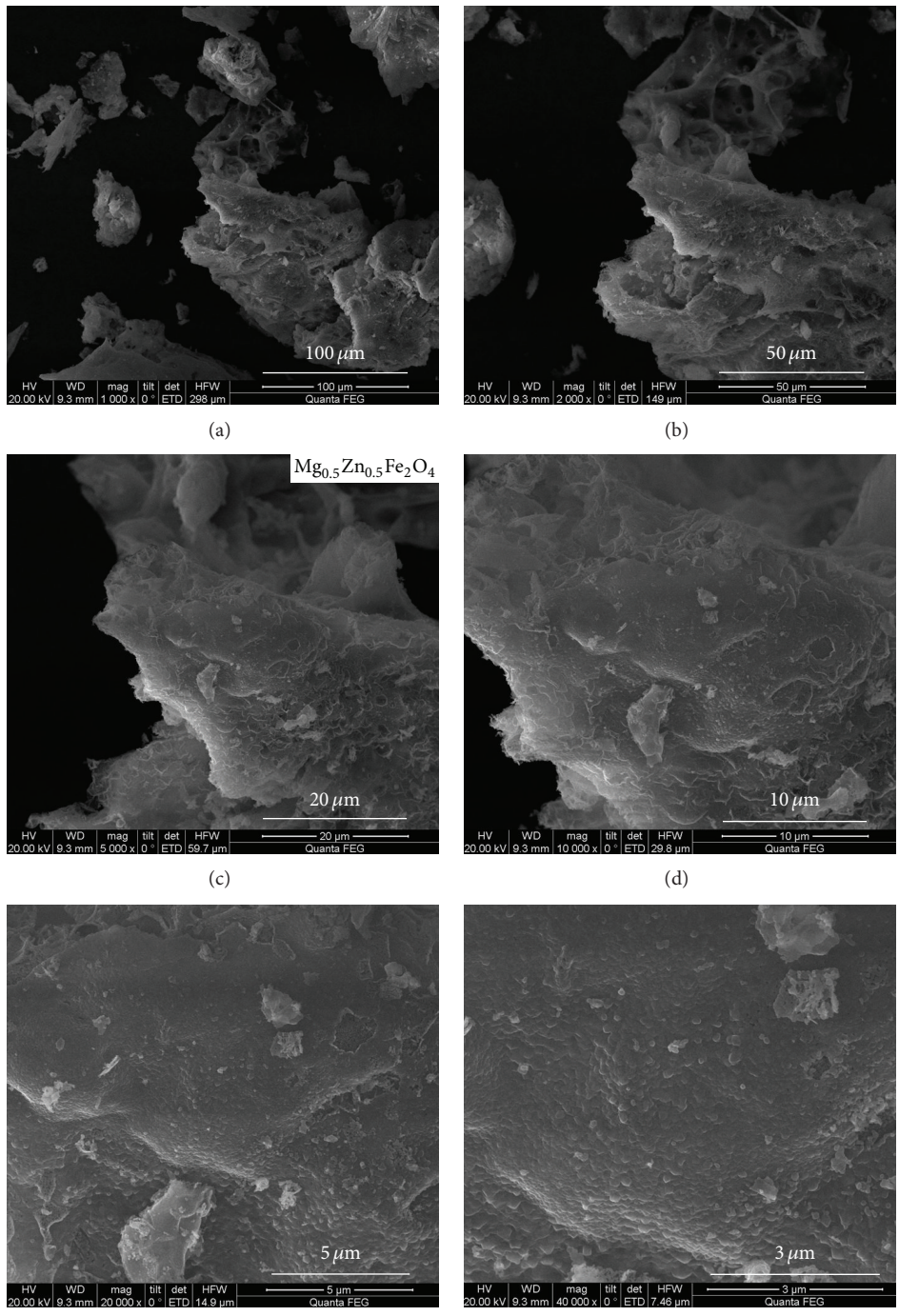

Figure 4: SEM micrographs depict $Mg_{0.5}Zn_{0.5}Fe_2O_4$ ferrites with diameters of 100 μm (a), 50 μm (b), 20 μm (c), 10 μm (d), 5 μm (e), and 3 μm (f).

site [3, 4, 10–12]. The magnetic moment n_B is expressed as [4, 5, 11].

$$\begin{aligned} n_B &= M_B - M_A = 5(1 + x + y) - 5(1 - x - y) \\ &= 10x + 10y, \end{aligned} \tag{3}$$

where M_B and M_A are the B and A sublattice magnetic moments. According to the literature [3], we assumed that the value of y is equal to 0.1. Figure 8 shows the change in experimental and theoretical magnetic moments with Zn content x.

From Figure 8, the experimental and theoretical magnetic moments increase as Zn content x increases. Furthermore, according to (3), the theoretical saturation magnetization increases with Zn content x increasing. The result of the experimental is in a good agreement with theoretical

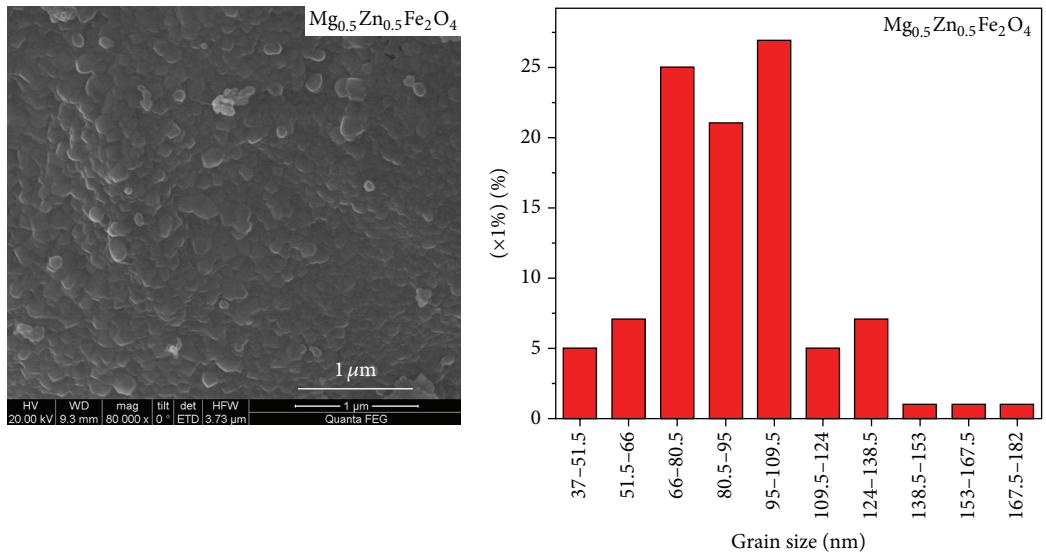

FIGURE 5: Histogram of grain size distribution of $Mg_{0.5}Zn_{0.5}Fe_2O_4$ ($x = 0.5$) annealed at 800°C.

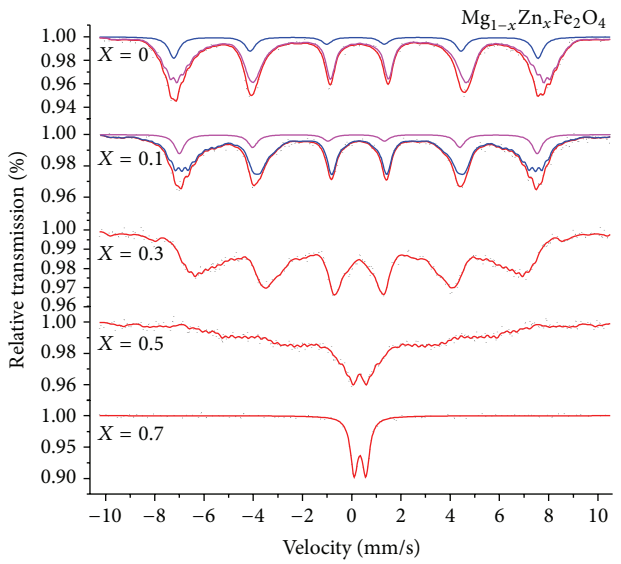

FIGURE 6: Room temperature Mössbauer spectra of $Mg_{1-x}Zn_xFe_2O_4$ annealed at 800°C.

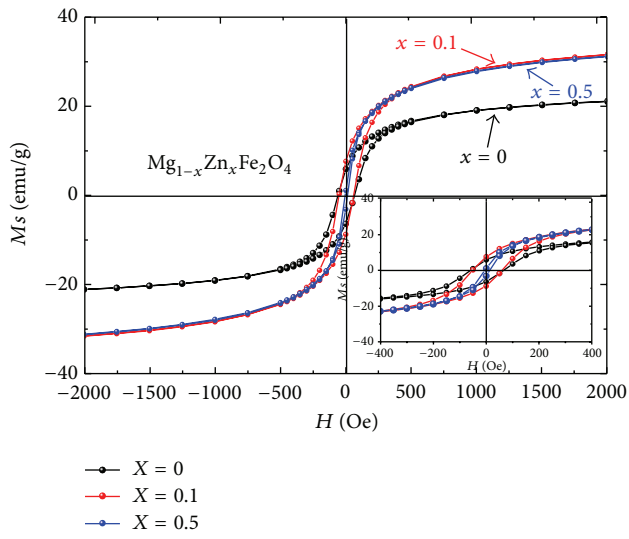

FIGURE 7: Room temperature hysteresis loops of $Mg_{1-x}Zn_xFe_2O_4$ annealed at 800°C.

saturation magnetization for all samples. However, the saturation magnetization of $Mg_{1-x}Zn_xFe_2O_4$ with $x = 0.1$ and 0.5 has no significant changes, maybe because the average grain size decreases with increasing Zn content from the SEM. It is known that porosity is inversely proportional, while the particle size is directly proportional to the magnetization for nanoferrites [24, 25].

It is observed from Table 3 that the coercivity of $Mg_{1-x}Zn_xFe_2O_4$ is less than 100 Oe, which indicating the all sample is soft magnetic materials. And the coercivity tends to decrease with Zn content x increasing. The magnetic coercivity of the particles depends significantly on their magnetocrystalline anisotropy, microstrain, interparticle interaction, temperature, size, and shape [9, 26, 27]. However the Zn^{2+} and Mg^{2+} ions have no unpaired electrons and lead to zero total electron spin. So replacing Mg^{2+} ions with the Zn^{2+} ions will not have much effect on the magnetic anisotropy constant. The reduction in magnetic coercivity is related to the grain size [28–30].

4. Conclusion

The analysis of XRD patterns for $Mg_{1-x}Zn_xFe_2O_4$ ($x = 0$, 0.1, 0.3, 0.5, 0.7) annealed at 800°C show that the increase in lattice constant is due to replacement of smaller Mg^{2+} ions

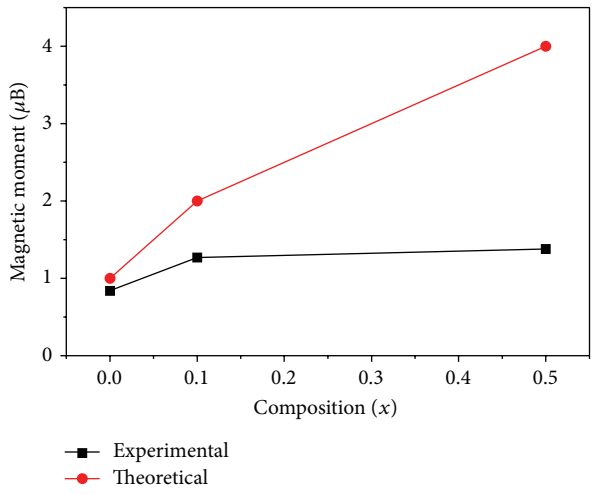

FIGURE 8: Variation in experimental and theoretical magnetic moment with zinc content x.

TABLE 3: Magnetic data for $Mg_{1-x}Zn_xFe_2O_4$ annealed at 800°C.

Sample (x)	M_S (emu/g)	H_C (Oe)	M_r (emu/g)	n_B
0	23.36	50.13	6.36	0.84
0.1	34.83	50.13	7.65	1.27
0.5	34.98	0.18	1.10	1.38

by larger Zn^{2+} ions. SEM results indicate the distribution of grains and morphology of the samples. Some particles are agglomerated due to the presence of magnetic interactions among particles. And the ferrite powers are nanoparticles. Room temperature Mössbauer spectra of $Mg_{1-x}Zn_xFe_2O_4$ display that the A Mössbauer absorption area decreases and the B Mössbauer absorption area increases with increasing zinc concentration. The change of the saturation magnetization can be explained with Néel's theory. The coercivity decreases with increasing Zn content is attributed to the grain size.

Conflict of Interests

The authors declare that they have no conflict of interests regarding this work.

Acknowledgments

This work was financially supported by the National Natural Science Foundation of China (nos. 11364004 and 11164002) and Innovation Project of Guangxi Graduate Education under Grant (no. 2010106020702M47).

References

[1] N. M. Deraz and A. Alarifi, "Novel preparation and properties of magnesioferrite nanoparticles," *Journal of Analytical and Applied Pyrolysis*, vol. 97, pp. 55–61, 2012.

[2] S. H. Hosseini and A. Asadnia, "Synthesis, characterization, and microwave-absorbing properties of polypyrrole/$MnFe_2O_4$ nanocomposite," *Journal of Nanomaterials*, vol. 2012, Article ID 198973, 6 pages, 2012.

[3] A. Franco Jr. and M. S. Silva, "High temperature magnetic properties of magnesium ferrite nanoparticles," *Journal of Applied Physics*, vol. 109, no. 7, Article ID 07B505, 2011.

[4] M. Manjurul Haque, M. Huq, and M. A. Hakim, "Effect of Zn^{2+} substitution on the magnetic properties of $Mg_{1-x}Zn_xFe_2O_4$ ferrites," *Physica B*, vol. 404, no. 21, pp. 3915–3921, 2009.

[5] M. M. Eltabey, A. M. Massoud, and C. Radu, "Microstructure and superparamagnetic properties of Mg-Ni-Cd ferrites nanoparticles," *Journal of Nanomaterials*, vol. 2014, Article ID 492832, 7 pages, 2014.

[6] A. Xia, S. Liu, C. Jin, L. Chen, and Y. Lv, "Hydrothermal $Mg_{1-x}Zn_xFe_2O_4$ spinel ferrites: phase formation and mechanism of saturation magnetization," *Materials Letters*, vol. 105, pp. 199–201, 2013.

[7] C. Choodamani, G. P. Nagabhushana, B. Rudraswamy, and G. T. Chandrappa, "Thermal effect on magnetic properties of Mg-Zn ferrite nanoparticles," *Materials Letters*, vol. 116, pp. 227–230, 2014.

[8] K. Verma, A. Kumar, and D. Varshney, "Dielectric relaxation behavior of $A_xCo_{1-x}Fe_2O_4$ (A = Zn, Mg) mixed ferrites," *Journal of Alloys and Compounds*, vol. 526, pp. 91–97, 2012.

[9] H. Mohseni, H. Shokrollahi, I. Sharifi, and K. Gheisari, "Magnetic and structural studies of the Mn-doped Mg-Zn ferrite nanoparticles synthesized by the glycine nitrate process," *Journal of Magnetism and Magnetic Materials*, vol. 324, no. 22, pp. 3741–3747, 2012.

[10] K. A. Mohammed, A. D. Al-Rawas, A. M. Gismelseed et al., "Infrared and structural studies of $Mg_{1-x}Zn_xFe_2O_4$ ferrites," *Physica B: Condensed Matter*, vol. 407, no. 4, pp. 795–804, 2012.

[11] B. Babić-Stojić, V. Jokanović, D. Milivojević et al., "Magnetic and structural studies of $CoFe_2O_4$ nanoparticles suspended in an organic liquid," *Journal of Nanomaterials*, vol. 2013, Article ID 741036, 9 pages, 2013.

[12] S. J. Haralkar, R. H. Kadam, S. S. More et al., "Substitutional effect of Cr^{3+} ions on the properties of Mg-Zn ferrite nanoparticles," *Physica B*, vol. 407, no. 21, pp. 4338–4346, 2012.

[13] W. A. A. Bayoumy, "Synthesis and characterization of nanocrystalline Zn-substituted Mg-Ni-Fe-Cr ferrites via surfactant-assisted route," *Journal of Molecular Structure*, vol. 1056-1057, pp. 285–291, 2014.

[14] S. Kanagesan, M. Hashim, S. Tamilselvan, N. B. Alitheen, I. Ismail, and G. Bahmanrokh, "Cytotoxic effect of nanocrystalline $MgFe_2O_4$ particles for cancer cure," *Journal of Nanomaterials*, vol. 2013, Article ID 865024, 8 pages, 2013.

[15] S. Hajarpour, K. Gheisari, and A. Honarbakhsh Raouf, "Characterization of nanocrystalline $Mg_{0.6}Zn_{0.4}Fe_2O_4$ soft ferrites synthesized by glycine-nitrate combustion process," *Journal of Magnetism and Magnetic Materials*, vol. 329, pp. 165–169, 2013.

[16] L. Bih, M. Azrour, B. Manoun, M. P. F. Graça, and M. A. Valente, "Raman spectroscopy, X-Ray, SEM, and DTA analysis of alkali-phosphate glasses containing WO_3 and Nb_2O_5," *Journal of Spectroscopy*, vol. 2013, Article ID 123519, 10 pages, 2013.

[17] Y. Zhang, J. Lin, and D. Wen, "Structure, infrared radiation properties and mössbauer spectroscopic investigations of $Co_{0.6}Zn_{0.4}Ni_xFe_{2-x}O_4$ ceramics," *Journal of Materials Science and Technology*, vol. 26, no. 8, pp. 687–692, 2010.

[18] M. Siddique and N. M. Butt, "Effect of particle size on degree of inversion in ferrites investigated by Mössbauer spectroscopy," *Physica B: Condensed Matter*, vol. 405, no. 19, pp. 4211–4215, 2010.

[19] S. Kumar, A. M. M. Farea, K. M. Batoo, C. G. Lee, B. H. Koo, and A. Yousef, "Mössbauer studies of $Co_{0.5}Cd_xFe_{2.5-x}O_4$ (0.0–0.5) ferrite," *Physica B*, vol. 403, no. 19-20, pp. 3604–3607, 2008.

[20] M. Gupta and B. S. Randhawa, "Mössbauer, magnetic and electric studies on mixed Rb-Zn ferrites prepared by solution combustion method," *Materials Chemistry and Physics*, vol. 130, no. 1-2, pp. 513–518, 2011.

[21] W. Bayoumi, "Structural and electrical properties of zinc-substituted cobalt ferrite," *Journal of Materials Science*, vol. 42, no. 19, pp. 8254–8261, 2007.

[22] M. V. Chaudhari, S. E. Shirsath, A. B. Kadam, R. H. Kadam, S. B. Shelke, and D. R. Mane, "Site occupancies of Co-Mg-Cr-Fe ions and their impact on the properties of $Co_{0.5}Mg_{0.5}Cr_xFe_{2-x}O_4$," *Journal of Alloys and Compounds*, vol. 552, pp. 443–450, 2013.

[23] X.-M. Liu and W.-L. Gao, "Preparation and magnetic properties of $NiFe_2O_4$ nanoparticles by modified pechini method," *Materials and Manufacturing Processes*, vol. 27, no. 9, pp. 905–909, 2012.

[24] S. Thankachan, B. P. Jacob, S. Xavier, and E. M. Mohammed, "Effect of neodymium substitution on structural and magnetic properties of magnesium ferrite nanoparticles," *Physica Scripta*, vol. 87, no. 2, Article ID 025701, 2013.

[25] Q. Lin, Z. Ye, C. Lei, H. Huang, Y. Xu, and Y. He, "Microstructure and magnetic research of NiCuZn ferrite by Co, Bi compound doped," *Materials Research Innovations*, vol. 17, no. 1, pp. 287–291, 2013.

[26] V. Lilkov, O. Petrov, Y. Tzvetanova, P. Savov, and M. Kadiyski, "Mössbauer, XRD, and complex thermal analysis of the hydration of cement with fly ash," *Journal of Spectroscopy*, vol. 2013, Article ID 231843, 9 pages, 2013.

[27] T. Jiao, Y. Wang, Q. Zhang et al., "Self-assembly and headgroup effect in nanostructured organogels via cationic amphiphile-graphene oxide composites," *PLoS ONE*, vol. 9, no. 7, Article ID e101620, 2014.

[28] J. Lin, Y. He, Q. Lin, R. Wang, and H. Chen, "Microstructural and Mössbauer spectroscopy studies of $Mg_{1-x}Zn_xFe_2O_4$ ($x = 0.57, 0.7$) nanoparticles," *Journal of Spectroscopy*, vol. 2014, Article ID 540319, 5 pages, 2014.

[29] M. J. Iqbal, Z. Ahmad, Y. Melikhov, and I. C. Nlebedim, "Effect of CuCr co-substitution on magnetic properties of nanocrystalline magnesium ferrite," *Journal of Magnetism and Magnetic Materials*, vol. 324, no. 6, pp. 1088–1094, 2012.

[30] T. Jiao, Q. Huang, Q. Zhang, D. Xiao, J. Zhou, and F. Gao, "Self-assembly of organogels via new luminol imide derivatives: diverse nanostructures and substituent chain effect," *Nanoscale Research Letters*, vol. 8, article 278, 2013.